Agnostic eXplainable Artificial Intelligence (XAI) Method Based on Volterra Series

Jhonatan Contreras[1,2,*,†] [a] and Thomas Bocklitz[1,2,*,†] [b]

[1] *Leibniz Institute of Photonic Technology, Albert Einstein Straße 9, 07745 Jena, Germany*

[2] *Institute of Physical Chemistry (IPC) and Abbe Center of Photonics (ACP), Friedrich Schiller University, Helmholtzweg 4, 07743 Jena, Germany*

Keywords: Explainabe Artificial Intelligence, Volterra Series, Model Approximation, Model Interpretation.

Abstract: Convolutional Neural Networks (CNN) have shown remarkable results in several fields in recent years. Traditional performance metrics assess model performance but fail to detect biases in datasets and models. Explainable artificial intelligence (XAI) methods aim to evaluate models, identify biases, and clarify model decisions. We propose an agnostic XAI method based on the Volterra series that approximates models. Our model architecture is composed of three second-order Volterra layers. Relevant information can be extracted from the model to be approximated and used to generate relevance maps that explain the contribution of the input elements to the prediction. Our Volterra-XAI learns its Volterra kernels comprehensively and is trained using a target model outcome. Therefore, no labels are required, and even when training data is unavailable, it is still possible to generate an approximation utilizing similar data. The trustworthiness of our method can be measured by considering the reliability of the Volterra approximation in comparison with the original model. We evaluate our XAI method for the classification task on 1D Raman spectra and 2D images using two common CNN architectures without hyperparameter tuning. We present relevance maps indicating higher and lower contributions to the approximation prediction (logit).

1 INTRODUCTION

The remarkable rise of convolutional neural networks (CNNs) makes them attractive for application in various fields, including the medical domain, where CNNs have been used to classify medical data successfully, such as Raman spectra, cystoscopy, and histological images (Lin et al., 2019)(Halicek et al., 2020)(Rodner et al., 2019) (Niioka et al., 2018). However, traditional accuracy metrics fail to detect (or can hide) biases in both datasets and models, which is critical in this sector. The models must be reliable and transparent. Therefore, explainable artificial intelligence (XAI) methods seek to describe the model behaviour using relevance maps, the notion of that class, and heat maps. Relevance maps (R-Map) specify the input elements that contribute the most to the classification output. The notion of that class indicates what the model expects as input to maximize a particular class. Heat maps (H-Map) show the features extracted by the model at different stages. The most popular XAI methods can be divided into three groups: perturbation-based (Mishra et al., 2017), which computes a set of duplicate inputs with perturbations (removing pixels or spectra) and evaluates how the prediction changes. Deconvolution-based (Lundberg and Lee, 2017), which generates salience maps using convolution transpose operations. Gradient-based (Simonyan et al., 2013), which uses backpropagation to calculate logit gradients to visualize the notion of the class.

Some XAI methods require access to model architecture and parameters, such as Integrated Gradient (Sundararajan et al., 2017), which utilizes an integral approximation by averaging gradients over a set of perturbed versions of the input image. Similarly, Taylor-based (Montavon et al., 2017) (TD) and Layer-wise Relevance Propagation (Bach et al., 2015) (LRP) produce relevance maps using partial derivatives of the model weights, requiring the model definition to backpropagate gradients.

[a] https://orcid.org/0000-0002-0491-9896

[b] https://orcid.org/0000-0003-2778-6624

*Member of Leibniz Health Technologies

†Member of the Leibniz Centre for Photonics in Infection Research (LPI)

Contreras, J. and Bocklitz, T.
Agnostic eXplainable Artificial Intelligence (XAI) Method Based on Volterra Series.
DOI: 10.5220/0011889700003411
In *Proceedings of the 12th International Conference on Pattern Recognition Applications and Methods (ICPRAM 2023)*, pages 597-606
ISBN: 978-989-758-626-2; ISSN: 2184-4313

Alternatively, XAI methods can be agnostic, indicating that they consider models a black box. For instance, a series of polynomial models derived from a Taylor expansion can approximate a non-linear model's output function (Bocklitz, 2019). Among the advantages of agnostic methods is their flexibility, which allows them to be applied to any AI model. A simpler and more explainable model increases the explainability. At the same time, it becomes more flexible by being able to choose a feature representation that may be different from the original model.

We propose an agnostic XAI method based on the Volterra series to approximate a target model (Korenberg and Hunter, 1996). In this manner, relevant information can be extracted to generate a relevance map that explains the contribution of the pixels to the prediction. Our Volterra-XAI learns its Volterra kernels comprehensively and is trained using the target model outcome. Therefore, no labels are required, and even when training data is unavailable, it is still possible to generate an approximation employing similar data. The relevance map is extracted from the second to last layer of the Volterra-XAI, and its trustworthiness can be measured by considering the reliability of the Volterra approximation. This value can be obtained from the difference between the outcome of the target model and the approximation model.

Section 2 and Section 3 introduce the Volterra series and Volterra Network. Section 4 presents the experiment protocol. Section 4.1 shows the result on a 1D dataset. Section 4.2 evaluates 2D models on the CIFAR 10 and the histology dataset. In all cases, our method compares some trained methods. Finally, Section 5 summarizes the contribution and set together the conclusions.

2 VOLTERRA SERIES

Consider a single-input, single-output (SISO) system with an input time function, $x(t)$, and output time function $y(t)$. This system can be, for example, an artificial intelligence method, such as a Linear Discriminant Analysis (LDA) model or a neural network. It can be extended in an infinite Volterra series as

$$y(t) = \sum_{i=0}^{\infty} V_i[h_i, x] \tag{1}$$

Where the zero-order Volterra term is a constant called the impulse response.

$$V_0[h_0, x] = h_0 \tag{2}$$

and for $i \geq 1$, the i-th-order Volterra term is

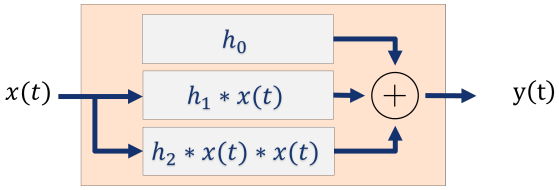

Figure 1: Visualization of the second-order Volterra series as block operation.

$$V_i[h_i, x] = \int_{-\infty}^{\infty} \cdots \int_{-\infty}^{\infty} h_i(\tau_1, \cdots, \tau_i) x(t-\tau_1) \cdots x(t-\tau_i) d_{\tau_1} \cdots d_{\tau_i} \tag{3}$$

Equations 1, 2 and 3 represent the Volterra series expansion, where the kernels h_i are the Volterra kernels (Stegmayer et al., 2004), (Korenberg and Hunter, 1996). Although the calculation of the Volterra kernels is a complicated and time-consuming task, several methods have been proposed (Stegmayer, 2004), (Azpicueta-Ruiz et al., 2010), (Franz and Schölkopf, 2006), (Orcioni, 2014) (Orcioni et al., 2018).

In this work, we propose an agnostic explainable artificial technique that approximates non-linear systems employing the second-order Volterra series, as shown in Equation 4 and Figure 1.

$$y(t) = h_0 + \int_{-\infty}^{\infty} h_1(\tau) x(t-\tau) d_\tau + \int_{-\infty}^{\infty} \int_{-\infty}^{\infty} h_2(\tau_1, \tau_2) x(t-\tau_1) x(t-\tau_2) d_{\tau_1} d_{\tau_2} \tag{4}$$

3 VOLTERRA NETWORK

Finding the kernels that satisfy the equation 4 is computationally expensive, and it is a problem similar to that faced by neural networks. Although it is theoretically possible to represent any possible function with a single Volterra expansion, we reduce the complexity by decomposing it into cascading layers, where each layer is a simpler Volterra series. Our Volterra layers are also second-order Volterra expansions, where one layer's output serves as the next layer's input. It reduces kernel sizes and helps learn more complex and abstract relationships in data.

Figure 2 shows the architecture of our feed-forward Volterra network. The base model has three Volterra layers, a tanh activation layer, and a dense layer with the c neurons corresponding to the number of classes of the respective task. The number of layers and kernels can be increased or decreased depending on the complexity of the data, the target model, and the task. In this paper, we present the results for 1D and 2D data. We do not perform hyperparameter optimization and use the same architecture to compare

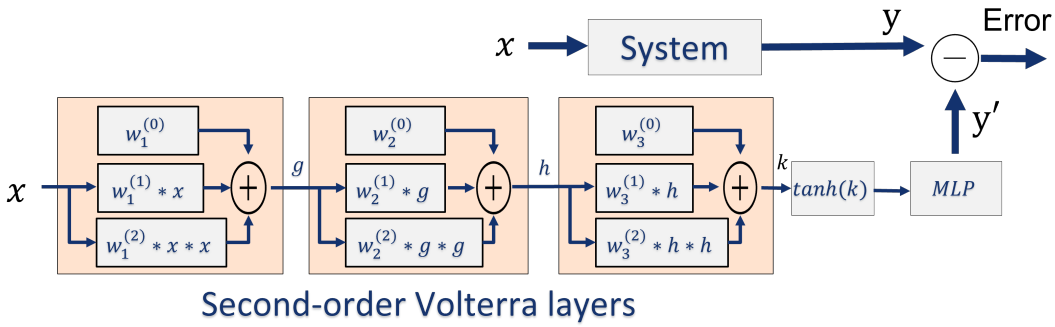

Figure 2: Architecture of our Volterra-XAI Network, composed of three Volterra layers, a tanh activation layer, and a dense layer with the c neurons corresponding to the number of classes of the respective task.

models. The following formulation can be extrapolated for the analysis of 2D images.

Let's define our 1D input vector x and a set of Volterra kernels $w = [w^{(0)}, w^{(1)}, w^{(2)}]$, and say that x has length n, $w^{(0)}$ has length 1, $w^{(1)}$ has length m, and $w^{(2)}$ has length mxm. The second-order Volterra approximation layer in the discrete domain can be defined as

$$y[n] = w^{(0)} + \sum_{i=1}^{m} w_i^{(1)} x[n-i] + \sum_{i=1}^{m} \sum_{j=1}^{m} w_{ij}^{(2)} x[n-i]x[n-j] \quad (5)$$

Therefore, the zero-order kernel $w^{(0)}$ corresponds to a learnable 1D tensor in our implementation, and the first-order kernel $w^{(1)}$ can be implemented as a discrete convolution operation, according to Equation 5. The second-order kernel $w^{(2)}$ requires the multiplication of the input signal, which can be implemented by defining a local multiplication in a sliding window.

The multiplication of the input signal can be efficiently implemented by local multiplications of sliding windows. Therefore, the input signal can be defined as a set of patches in the form $x = [x_1, x_2, ..., x_m]$. Therefore, we can reformulate Equation 5 as following:

$$y(x) = w^{(0)} + \sum_{i=1}^{m} w_i^{(1)} x_i + \sum_{i=1}^{m} \sum_{j=1}^{m} w_{ij}^{(2)} x_i x_j \quad (6)$$

In matrix notations, the kernel $w^{(2)}$ has a dimension of $(mxm, 1)$. The second term of Equation 6 can be replaced by the Khatri-Rao product (Khatri and Rao, 1968), (Seber, 2008), which is the column-wise Kronecker product of two matrices. Given a $M \times N$ matrix A and a $P \times Q$ matrix B, Khatri-Rao product $A \odot B$ has size $MP \times N$ is given by

$$A \odot B = [a_1 \otimes b_1 \quad a_2 \otimes b_2 \quad \cdots \quad a_N \otimes b_N] \quad (7)$$

Where the Kronecker product (Seber, 2008) is denoted by $\otimes$, given the matrices $M \times N$ matrix A and a $P \times Q$ matrix B, the Kronecker product $A \otimes B$ has size $MP \times NQ$ is given by

$$A \otimes B = \begin{bmatrix} a_{11}B & a_{12}B & \cdots & a_{1N}B \\ a_{21}B & a_{22}B & \cdots & a_{2N}B \\ \vdots & \vdots & \ddots & \vdots \\ a_{M1}B & a_{M2}B & \cdots & a_{MN}B \end{bmatrix} \quad (8)$$

Therefore, the Equation 6 can be rewrite as

$$y(x) = w^{(0)} + (w^{(1)})^T x + (w^{(2)})^T (x \otimes x) \quad (9)$$

4 EXPERIMENTS

We evaluate our XAI method for the classification task, in this particular case, for Raman spectra and 2D images. For the experiments, we present models that obtain training, validation, and test accuracy relatively close to state-of-the-art without hyperparameter tuning. Parameter selection and accuracy could be improved with a more sophisticated hyperparameter search, a learning rate program, a different optimizer, or even more modern models. However, our goal is not to train the best model but to agnostically evaluate the trained models and provide insights to scientists with extensive knowledge in areas other than data science, such as medicine, chemistry, and physics.

4.1 Raman Spectra

Dataset. This Raman-spectral data set contains six bacterial species, including Escherichia coli DSM 423, Klebsiella terrigena DSM 2687, Pseudomonas stutzeri DSM 5190, Listeria innocua DSM 20649, Staphylococcus warneri DSM 20316, and Staphylococcus cohnii DSM 20261, from Deutsche Sammlung von Mikroorganismen and Zellkulturen GmbH (DSMZ) (Ali et al., 2018). The dataset contains 5420

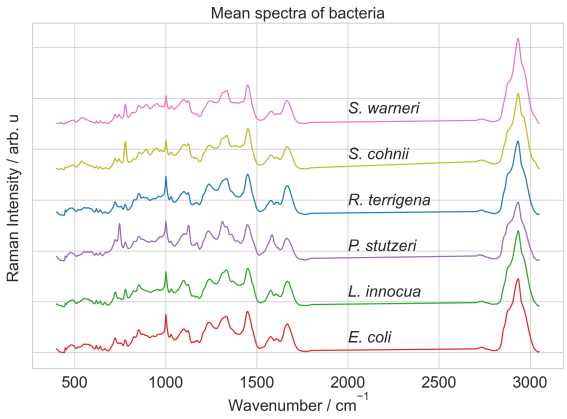

Figure 3: Mean spectra of bacteria dataset.

preprocessed spectra with 584 wavenumbers, Figure 3 shows the mean spectra for each class.

The preprocessing consists of cosmic spikes removal, wavenumber calibration, spectra aligned between 240–3190 cm–1, and baseline correction. All species were cultivated in nine independent biological replicates (batches). Accordingly, we evaluated by cross-validation, where the test set is composed of two batches, and the remaining (7 batches) are used for training (70%) and validation (30%).

We compare two CNN models trained from scratch, a traditional 1D CNN and a transformer base model (TrCNN) (Vaswani et al., 2017). The CNN comprises a feature extraction part (convolutional layers) and the classification part (dense layers). The TrCNN comprises multi-head attention layers for feature extraction and dense layers for classification.

Table 1 presents both models' mean sensitivity obtained for cross-validation on a total of 36 models. The CNN model has a mean sensitivity of 83.05% with a standard deviation of 4.08%, while the mean sensitivity of the TrCNN was 82.06% with a standard deviation of 5.34%.

Table 1: Sensitivities of all classes for the first fold in Percent (%). Cross-validation mean sensitivity for the CNN and Transformer (TrCNN) model.

Class	CNN		TrCNN	
	Test	Train	Test	Train
E. coli	68.87	100	51.53	92.0
L. innocua	97.57	100	96.60	90.0
P. stutzeri	88.00	100	80.00	100.0
R. terrigena	57.84	100	88.23	94.12
S. cohnii	93.93	100	84.84	98.11
S. warneri	89.10	100	89.60	97.10
AVG Sens	82.55	100	81.80	95.22
CV-Mean Sens	83.05± 4.08		82.06±5.34	

Table 2: Mean absolute error (MAE) of the logits expresses the difference between a target model and the Volterra approximation on the bacteria spectra dataset. The number of parameters for the target models and Volterra network.

Model	CNN	TrCNN
MAE Train	0.5040	0.2174
MAE Validation	1.3211	0.4119
MAE Test	1.2521	0.3874
Model parameters	19.5M	104.4K
Volterra parameters	175.2K	175.2K

Table 1 also reports the average and the sensitivity of all classes for the first fold. The average sensitivity of batch 0 is close to the mean cross-validation sensitivity, indicating that it is a successfully trained model. The traditional 1D CNN performs slightly better. Nevertheless, note that the number of CNN parameters used is significantly higher (19.5 M) than the TrCNN model parameters (104.4 K), as shown in table 2.

4.1.1 1D Volterra Approximation

We evaluate the models trained on the first fold using our Volterra method. Although the models have different architectures and parameters, we used the same architecture in our Volterra network to approximate both models. A better approximation can be found by parameter selection. The tanh activation function at the last Volterra layer transforms the output values from -1 to 1. These values are combined linearly using a dense layer to approximate the logit values of the original models. This linear combination can be visualized as a relevance map or saliency map.

Table 2 exhibits the approximation error, which is the difference between the target model output and the Volterra approximation. As expected, the errors of the transformer model (Tr-CNN) are much lower. This model has fewer parameters and has a slightly lower performance than the CNN model, with 104.4K parameters, while the CNN has 19.5M parameters. The two Volterra models are identical. The approximation error can be reduced by increasing the number of parameters, layers, or training strategies.

Figure 4 shows examples of two saliency maps for the CNN model generated using our Volterra approximation and a Taylor-based (Montavon et al., 2017) method. Each saliency map is divided into two sections. The top part corresponds to the classifier prediction, and the bottom corresponds to the ground truth class.

The spectra in Figure 4a correspond to the *E. coli* class, but is wrongly classified as *R. terrigena*. Correctly classified spectra have equal saliency maps, as

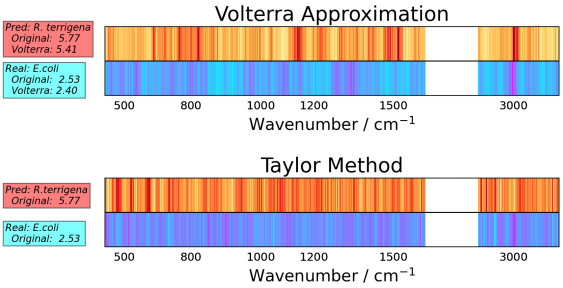

a. Wrongly classified spectra.

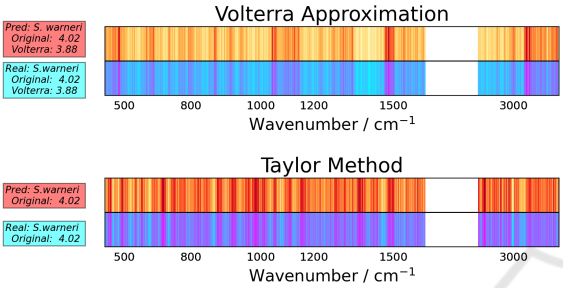

b. Correctly classified spectra.

Figure 4: Saliency Map for the CNN model generated using the Volterra approximation (top) and a Taylor-based (Montavon et al., 2017) method (bottom). Each saliency map is divided into two sections. The top part corresponds to the classifier prediction, and the bottom corresponds to the ground truth class.

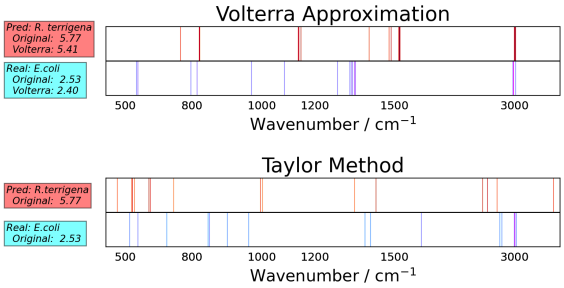

a. Wrongly classified spectra.

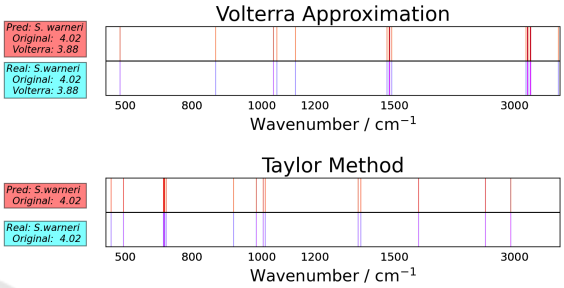

b. Correctly classified spectra.

Figure 5: K most relevant wavenumber postions (variables) for the CNN model obtained using our Volterra method (top) and the Taylor method (bottom). Each saliency map is divided into two sections. The top part corresponds to the classifier prediction, and the bottom corresponds to the ground truth class.

shown in Figure 4b. For the predicted class, the areas with dark red are the areas that influence the most, while the areas in yellow are less important for the classification. Simultaneously, for the correct class, the bands that influence the most are magenta, and the bands that influence the least are cyan.

The Volterra approximation error is an indicator of the saliency map quality. A small error indicates that the input is close to the expected spectra for that class. The information provided for saliency maps is difficult to read, especially for the Taylor method, which displays excessive noise. We can see that the result does not focus on the areas as our method does.

We consider that a better manner to examine this output is to focus only on the k most relevant wavenumbers. Figure 5 shows the top 15 spectra (wavenumbers) for the CNN model obtained using our Volterra method (top) and the Taylor method (bottom). Figure 5a shows an example of a misclassified spectrum. The spectra in Figure 5b were correctly classified, and the difference between the target model output and the Volterra approximation is 0.07, which corresponds to 2.25%.

Figure 6 shows histograms constructed using the training data, which accumulate the k most important wavenumbers for two classes (*E. coli* and *L. innocua*).

The red areas indicate the most frequently used bands by the classifier according to the Volterra and Taylor-based methods.

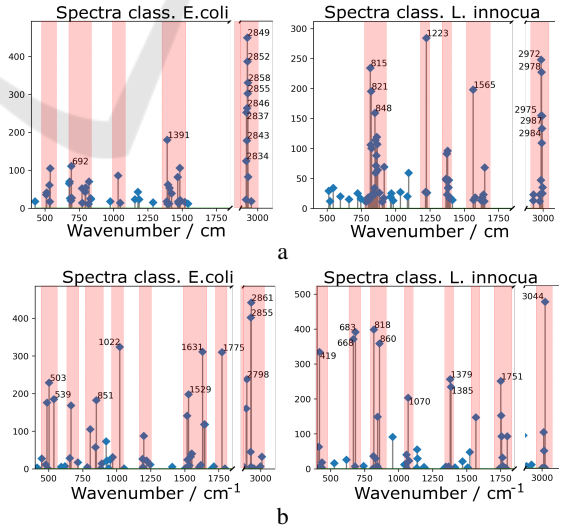

Figure 6: Histograms accumulate the kth most important wavenumbers for the CNN model. (a) Volterra approximation, (b) Taylor-based method. The red areas indicate the most frequently used bands by the CNN model.

The bands shown by the Volterra model are more concentrated, while the bands used by the Taylor method are highly distributed. Taylor-based models should theoretically select a root point value; by approximating this value, the results are only guaranteed stable for some cases. Some recent variations of the Taylor method, such as layer-wise backpropagation, employ rules to select a reference point and to omit negative gradients or enhance positive ones. However, there needs to be a defined way to establish whether the generated map is reliable. On the other hand, in this work, we use the Volterra approximation to state directly the cases in which our model deviates too much from the original model, so the result should not be considered.

4.2 2D Images

We assess our 2D Volterra model on two datasets, CIFAR-10 (Krizhevsky et al., 2009), and a public histology dataset (Kather et al., 2016). Hundreds of methods are used for image classification. In this paper, we select two models, a popular transfer learning strategy and a transformer-based network in the top 5 state-of-the-art. Both models can be improved by changing the architecture, increasing the number of layers, by parameters such as the learning rate schedule, optimizer, weight decay, or data augmentation. However, our interest is not to train the best network, but to evaluate previously trained networks.

Transfer learning. This CNN network performs transfer learning based on one of the most common pre-trained networks, the ResNet50, available in Keras, where the weights are pre-trained in Imagenet. All layers are retained except the final classification layers, replaced by two dense layers with non-linear activation ReLU and the last layer with Softmax activation.

Transformer-based network. We implemented TrCNN, a version of the Vision Transformer (ViT) model proposed by (Dosovitskiy et al., 2020) for image classification. TrCNN uses the self-attentive Transformer architecture, which requires images to be transformed into patch sequences.

4.2.1 CIFAR-10

CIFAR-10 is a benchmark dataset consisting of 60000 32×32 color images in 10 classes, with 6000 images per class, including airplanes, cars, birds, cats, deer, dogs, frogs, horses, ships, and trucks. There are 50000 training images and 10000 test images. The training dataset is divided into validation (20%) and training (80%) splits in our experiments. The test split contains 1000 images from each class.

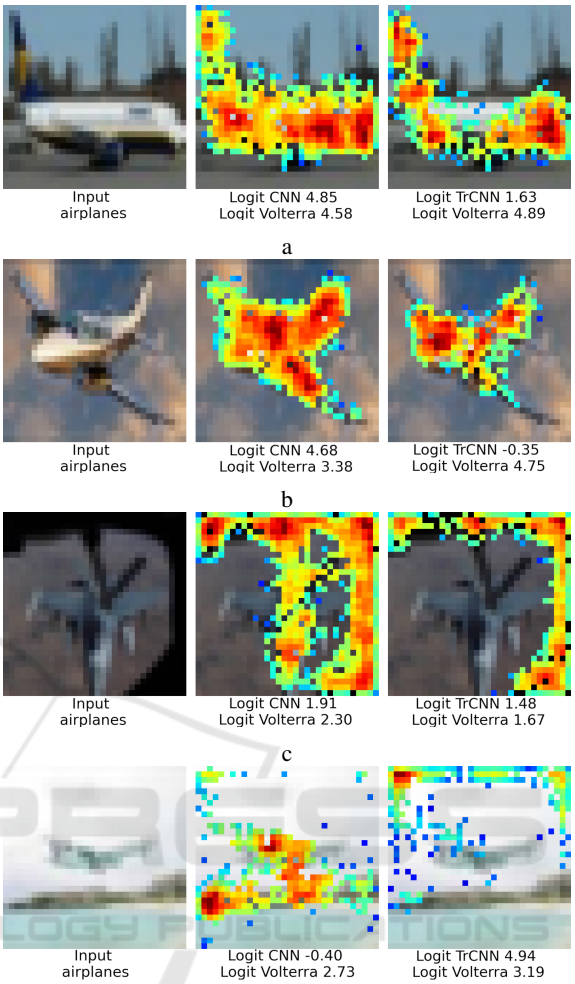

Figure 7: Relevance maps and logit values for the airplane class. (a-b) correct classification, the error is small (relevance maps can be trusted). (c) correct classification. However, the pixels used for the estimation are incorrect. (d) incorrect classification, the error is large (the relevance map cannot be trusted).

Table 3: Classification results for CIFAR 10 dataset, mean accuracy, top-5 accuracy. The number of parameters for the target models and Volterra network.

Model	CNN	TrCNN
Mean Accuracy	82.95	64.18
Top-5 Accuracy	99.12	96.26
Model Parameters	26.1M	507.2K
Volterra Parameters	1.4M	1.4M

Table 3 shows the classification mean accuracy and top-5 accuracies. The accuracy for CNN (transfer learning, Resnet-50) is lower than the typical value of around 90%, obtained through a better learning rate

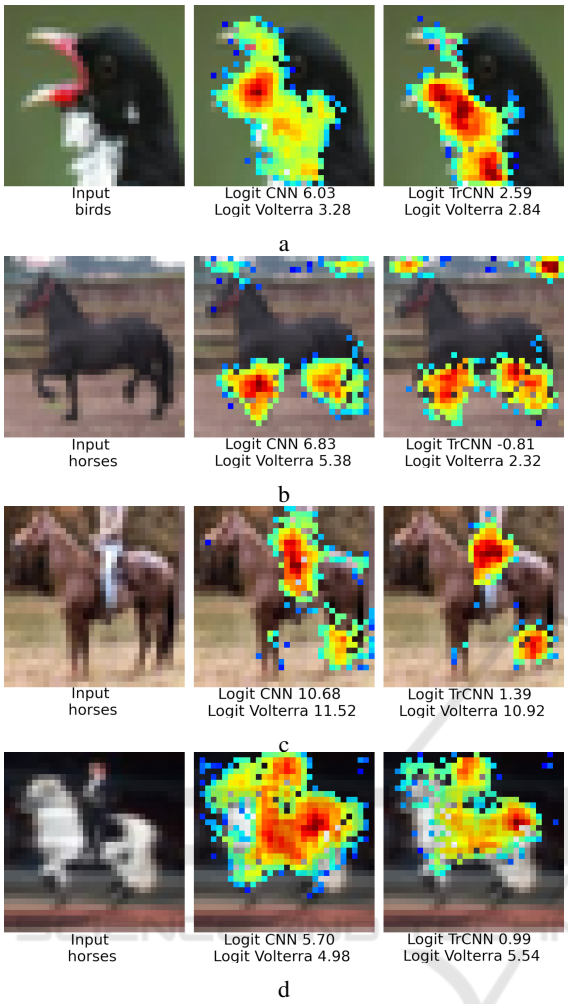

Figure 8: Relevance maps and logit values for CNN model and Volterra method for the CIFAR 10 dataset.

selection and a robust data augmentation strategy.

On the other hand, Alexey Dosovitskiy et al. (Dosovitskiy et al., 2020) reported an accuracy of 99.5% achieved by pre-training the ViT model using the JFT-300M dataset, then fine-tuning it on CIFAR 10, in our case, we trained the network from scratch, obtaining only accuracy of 64.18% and top 5 accuracies of 96.26% as shown in Table 3.

Table 4 summarizes the logit errors.

Table 4: Mean absolute error of the logits on CIFAR 10 dataset, which expresses the difference between the models and the Volterra approximation.

Model	Train	Validation	Test
CNN	0.5040	1.3211	1.2521
TrCNN	0.2174	0.4119	0.3874

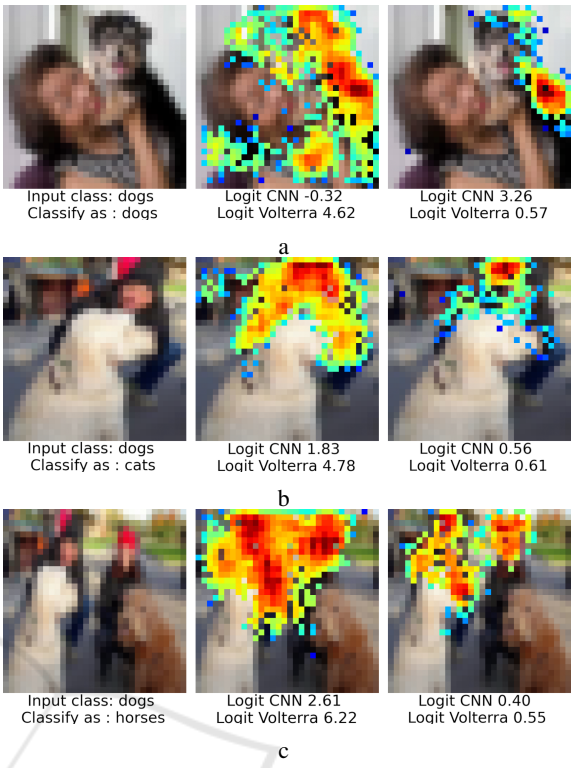

Figure 9: Relevance maps and logit values for the CNN model and Volterra method for the class dog.

We employ the mean absolute error to measure the difference between the models and the Volterra approximation logits, which have a dynamic range.

The CNN error is greater than the error for the TrCNN, because it is more complex, with 26.1M parameters, while TrCNN has just 500K, and our Volterra network uses only 1.4M.

Figure 7 shows relevance maps obtained using our Volterra method for images of the airplane class. The logit for the CNN, TrCNN, and the Volterra approximation method. The larger the logit value for the original model, the more it indicates that the class is an airplane. The prediction of the original model for Figure 7a and Figure 7b are correct. We can observe that the pixels that belong to the planes are shown with more intensity. Consequently, the model is paying attention to the right place. Additionally, the Volterra approximation error is small. Therefore, the relevance map can be trusted. The classification of Figure 7c is correct. However, the relevance map shows that the classification is based on the shape of the black pixels at the edge of the image, which are artifacts and possibly correspond to the window from which the picture was taken. The original model's prediction in Figure 7d is incorrect. The logit corresponding to the class airplane is negative, and the model classified it as a

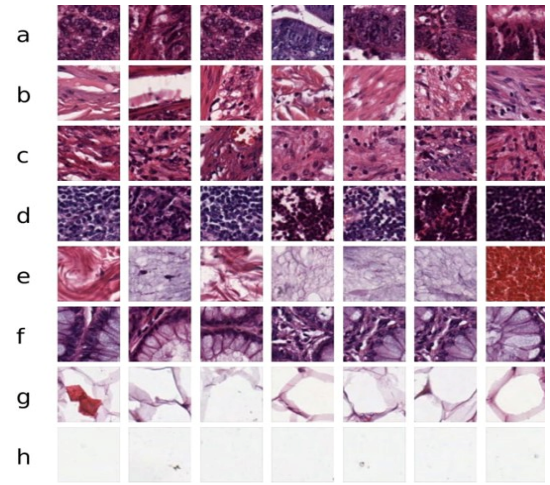

Figure 10: Images of every tissue class from the stained colorectal cancer histology dataset (Kather et al., 2016). (a) tumour epithelium, (b) simple stroma, (c) complex stroma, (d) immune cell conglomerates, (e) debris and mucus, (f) mucosal glands, (g) adipose tissue, and (h) background.

ship. In this case, the highlighted pixels belong to the background (sky and mountains). Fortunately, we can use this large Volterra approximation error to indicate that this relevance map should not be trusted.

Figure 8 shows additional relevance maps for correct predictions of images for the classes bird and horse. Figure 8c and Figure 8d show that humans are the most relevant pixels to classify these images as horses. However, humans are not present in CIFAR-10 as a class, but there are several images where they ride horses, showing a clear example of bias.

Figure 9 shows tested images not from the dataset, with humans and dogs. Dogs are correctly classified if humans are next to them, as shown in Figure 9a. However, when the humans are on top, the classifier gets confused, and some are classified as horses. Figure 9b is correctly classified. However, the model is almost equally confident that the image is a dog or a horse with logit values equal to 4.08 and 3.10. Figure 9c is classified as a horse, which shows that the relevance maps in Figure 9 classify were correct.

4.2.2 Colorectal Dataset

The H&E stained colorectal cancer histology dataset (Kather et al., 2016) has eight different classes: tumor epithelium, simple stroma, complex stroma (stroma containing single tumor cells and/or single immune cells), immune cell conglomerates, debris and mucus, mucosal glands, adipose tissue, and background. The images are tissue tiles at different scales ranging from individual cells, with an approximate size of 10 µm, e.g., Figure 10 (d) to larger structures such as mucosal glands $\geq$ 50 µm, e.g., Figure 10 (f). The dataset has 5000 images, 3200 were used for training, 800 for validation, and 1000 for testing. The size of the RGB images is 224×224. The models were trained from scratch without data augmentation during 200 epochs.

Table 5: Accuracy on stained histology dataset (in Percent), number of parameters for the target models and Volterra network.

Model	CNN	TrCNN
Accuracy	92.4	79.20
Model Parameters	26.2M	703.6K
Volterra Parameters	6.4M	6.4M

Table 6: Mean absolute error (MAE) of the logits expresses the difference between a target model and the Volterra approximation on the stained histology dataset.

Model	Train	Validation	Test
CNN	0.0108	0.0636	0.0617
TrCNN	0.0114	0.1013	0.0992

Table 5 shows the mean accuracy and the number of parameters for the CNN, TrCNN, and Volterra network. The CNN accuracy is significantly higher than the TrCNN model. Although TrCNN is a newer and state-of-the-art model, this network is trained from scratch and has no pre-training. The results for both models can be improved using different strategies. However, our interest is to analyze trained models.

Table 6 presents the approximation mean absolute error, which measures the difference between the models and their Volterra approximation. The errors are low, and the validation and testing errors are in the same range and not too far from the training error. We use identical Volterra models even though the models are different. The Volterra model can be more or less complex if a more precise approximation is required. However, the approximation found is satisfactory.

Figure 11 displays relevance maps obtained by our method on the CNN and TrCNN. In most cases, Volterra's logit is remarkably close to the target model. In the relevance maps, dark blue indicates that the pixels are less influential, and red indicates greater relevance. Background class, and some tissues such as debris and mucus (see Figure 11d), contain homogeneous texture, so the relevance is distributed throughout the image, except for some areas in red that break homogeneity. Figure 11b and Figure 11c are opposite, while Figure 11b should highlight only the stroma (note that the relevance map indicates in blue that cells are being ignored). Figure 11c should omit the stroma and look at the immune cell conglomerates.

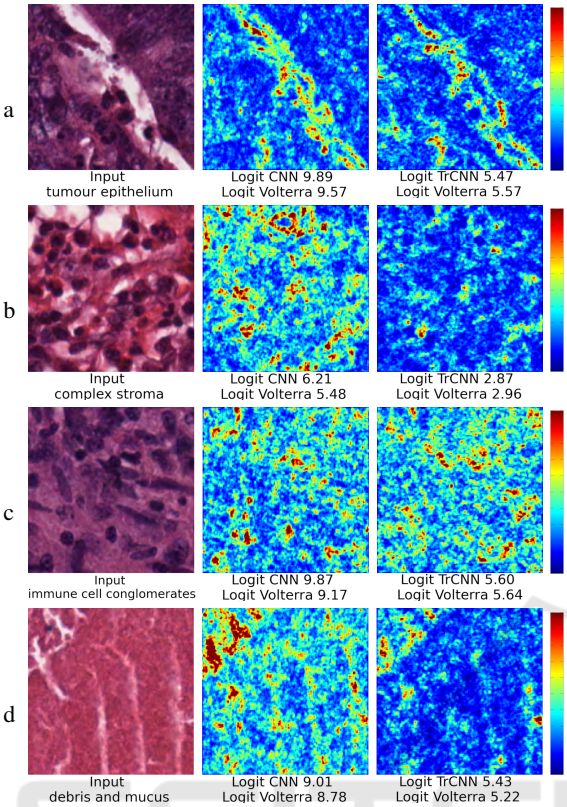

Figure 11: Histology dataset, relevance maps and logits (a) tumour epithelium, (b) complex stroma, (c) immune cell conglomerates, and (d) debris and mucus.

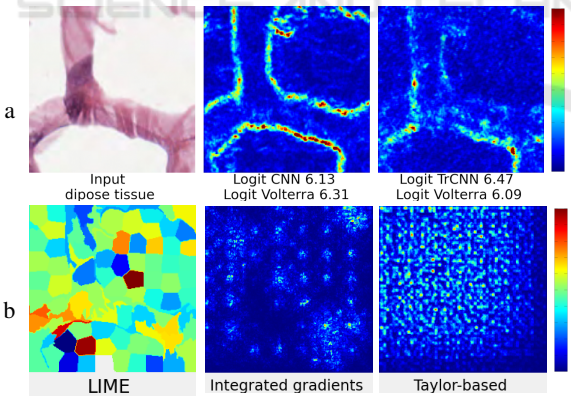

Figure 12: Histology dataset, explanations for adipose tissue. (a) Input and Volterra relevance maps, (b) Comparison with existing approaches.

Figure 12 compares the relevance map obtained for our Volterra XAI method and other existing approaches for adipose tissue. Texture and color are not relevant to our method for the lipid class (see Figure 12a). The edges of the lipids that form structures and lines allow this class to be classified. In contrast, LIME (Mishra et al., 2017) exhibits an output with few details because it is based on the search for relevant regions. The results obtained by integrated gradients (Sundararajan et al., 2017) and Taylor-based (Montavon et al., 2017) method are hardly interpretable. Gradient methods describe pixel changes in the model's prediction and do not fully explain the model prediction. Alternatively, Volterra relevance maps can be used directly by more experienced users (physicians) who can check the models for biases.

5 CONCLUSIONS

We propose an agnostic explainable artificial intelligence method based on the Volterra series to approximate models, identify biases, and clarify model decisions. The model architecture is composed of second-order Volterra layers. To make fair comparisons from our point of view, we used identical Volterra models even though the target models were different. However, the Volterra model can be more or less complex if a more precise approximation is required. Our Volterra network allows us to create a simpler model by emulating a target model. We evaluate the performance of the emulation numerically by comparing a target model's prediction and the Volterra approximation. Therefore, no labels are required, and comparable data can be employed even when training data is unavailable. We generate relevance maps for Raman spectra and 2D images. They explain the contribution of the input elements to the prediction. The trustworthiness of our method can be measured by considering the error of the Volterra approximation. We obtain low training errors for most of the models. The validation and testing errors are in the same range and not too far from the training error for the bacteria dataset (TrCNN), histology dataset (CNN and TrCNN), and CIFAR 10 (TrCNN). We present relevance maps indicating higher and lower contributions to the approximation prediction (logit) for commonly used models. We identify biases in the models trained on the CIFAR 10 dataset, which allows us to eliminate them. Despite this does not seem transcendental for the classification of simple classes, bias identification is critical in the medial area.

ACKNOWLEDGEMENTS

This work is supported by the Ministry for Economics, Sciences and Digital Society of Thuringia (TMWWDG), under the framework of the Landesprogramm ProDigital (DigLeben-5575/10-9) and the Federal Ministry of Education and Research

of Germany (BMBF), funding program Photonics Research Germany (FKZ: 13N15466, 13N15710, 13N15708) and is integrated into the Leibniz Center for Photonics in Infection Research (LPI). The LPI initiated by Leibniz-IPHT, Leibniz-HKI, UKJ and FSU Jena is part of the BMBF national roadmap for research infrastructures.

REFERENCES

Ali, N., Girnus, S., Rösch, P., Popp, J., and Bocklitz, T. (2018). Sample-size planning for multivariate data: a raman-spectroscopy-based example. *Analytical chemistry*, 90(21):12485–12492.

Azpicueta-Ruiz, L. A., Zeller, M., Figueiras-Vidal, A. R., Arenas-Garcia, J., and Kellermann, W. (2010). Adaptive combination of volterra kernels and its application to nonlinear acoustic echo cancellation. *IEEE Transactions on Audio, Speech, and Language Processing*, 19(1):97–110.

Bach, S., Binder, A., Montavon, G., Klauschen, F., Müller, K.-R., and Samek, W. (2015). On pixel-wise explanations for non-linear classifier decisions by layer-wise relevance propagation. *PloS one*, 10(7):e0130140.

Bocklitz, T. (2019). Understanding of non-linear parametric regression and classification models: A taylor series based approach. In *ICPRAM*, pages 874–880.

Dosovitskiy, A., Beyer, L., Kolesnikov, A., Weissenborn, D., Zhai, X., Unterthiner, T., Dehghani, M., Minderer, M., Heigold, G., Gelly, S., et al. (2020). An image is worth 16x16 words: Transformers for image recognition at scale. *arXiv preprint arXiv:2010.11929*.

Franz, M. O. and Schölkopf, B. (2006). A unifying view of wiener and volterra theory and polynomial kernel regression. *Neural computation*, 18(12):3097–3118.

Halicek, M., Dormer, J. D., Little, J. V., Chen, A. Y., and Fei, B. (2020). Tumor detection of the thyroid and salivary glands using hyperspectral imaging and deep learning. *Biomedical Optics Express*, 11(3):1383–1400.

Kather, J. N., Weis, C.-A., Bianconi, F., Melchers, S. M., Schad, L. R., Gaiser, T., Marx, A., and Zöllner, F. G. (2016). Multi-class texture analysis in colorectal cancer histology. *Scientific reports*, 6(1):1–11.

Khatri, C. and Rao, C. R. (1968). Solutions to some functional equations and their applications to characterization of probability distributions. *Sankhyā: The Indian Journal of Statistics, Series A*, pages 167–180.

Korenberg, M. J. and Hunter, I. W. (1996). The identification of nonlinear biological systems: Volterra kernel approaches. *Annals of biomedical engineering*, 24(2):250–268.

Krizhevsky, A., Hinton, G., et al. (2009). Learning multiple layers of features from tiny images.

Lin, H., Deng, F., Zhang, C., Zong, C., and Cheng, J.-X. (2019). Deep learning spectroscopic stimulated raman scattering microscopy. In *Multiphoton Microscopy in the Biomedical Sciences XIX*, volume 10882, pages 207–214. SPIE.

Lundberg, S. M. and Lee, S.-I. (2017). A unified approach to interpreting model predictions. *Advances in neural information processing systems*, 30.

Mishra, S., Sturm, B. L., and Dixon, S. (2017). Local interpretable model-agnostic explanations for music content analysis. In *ISMIR*, volume 53, pages 537–543.

Montavon, G., Lapuschkin, S., Binder, A., Samek, W., and Müller, K.-R. (2017). Explaining nonlinear classification decisions with deep taylor decomposition. *Pattern recognition*, 65:211–222.

Niioka, H., Asatani, S., Yoshimura, A., Ohigashi, H., Tagawa, S., and Miyake, J. (2018). Classification of c2c12 cells at differentiation by convolutional neural network of deep learning using phase contrast images. *Human cell*, 31(1):87–93.

Orcioni, S. (2014). Improving the approximation ability of volterra series identified with a cross-correlation method. *Nonlinear Dynamics*, 78(4):2861–2869.

Orcioni, S., Terenzi, A., Cecchi, S., Piazza, F., and Carini, A. (2018). Identification of volterra models of tube audio devices using multiple-variance method. *Journal of the Audio Engineering Society*, 66(10):823–838.

Rodner, E., Bocklitz, T., von Eggeling, F., Ernst, G., Chernavskaia, O., Popp, J., Denzler, J., and Guntinas-Lichius, O. (2019). Fully convolutional networks in multimodal nonlinear microscopy images for automated detection of head and neck carcinoma: Pilot study. *Head & neck*, 41(1):116–121.

Seber, G. A. (2008). *A matrix handbook for statisticians*. John Wiley & Sons.

Simonyan, K., Vedaldi, A., and Zisserman, A. (2013). Deep inside convolutional networks: Visualising image classification models and saliency maps. *arXiv preprint arXiv:1312.6034*.

Stegmayer, G. (2004). Volterra series and neural networks to model an electronic device nonlinear behavior. In *2004 IEEE International Joint Conference on Neural Networks (IEEE Cat. No. 04CH37541)*, volume 4, pages 2907–2910. IEEE.

Stegmayer, G., Pirola, M., Orengo, G., and Chiotti, O. (2004). Towards a volterra series representation from a neural network model. *WSEAS Transactions on Systems*, 3(2):432–437.

Sundararajan, M., Taly, A., and Yan, Q. (2017). Axiomatic attribution for deep networks. In *International conference on machine learning*, pages 3319–3328. PMLR.

Vaswani, A., Shazeer, N., Parmar, N., Uszkoreit, J., Jones, L., Gomez, A. N., Kaiser, Ł., and Polosukhin, I. (2017). Attention is all you need. *Advances in neural information processing systems*, 30.